Environmental Science and Pollution Research (2018) 25:19122–19133
https://doi.org/10.1007/s11356-018-2114-z

RESEARCH ARTICLE

In situ synthesis of g-C_3N_4/TiO_2 heterojunction nanocomposites as a highly active photocatalyst for the degradation of Orange II under visible light irradiation

Bin Ren[1] · Tiecheng Wang[1,2] · Guangzhou Qu[1,2] · Fang Deng[3] · Dongli Liang[1,2] · Wenli Yang[1] · Meishan Liu[1]

Received: 5 January 2018 / Accepted: 23 April 2018 / Published online: 4 May 2018

Abstract

As a highly active photocatalyst, g-C_3N_4/TiO_2 heterojunction nanocomposites were in situ synthesized by simple ultrasonic mixing and calcination by using TiO_2 and melamine as precursors. The morphology and structure of the prepared photocatalysts were characterized by field emission scanning electron microscopy, transmission electron microscopy, X-ray diffraction, Fourier-transform infrared spectroscopy, UV-Vis diffuse reflectance spectroscopy, and X-ray photoelectron spectroscopy. The photocatalytic activities of g-C_3N_4/TiO_2 nanocomposites to degrade Orange II (AO7) under visible light irradiation were evaluated. Results showed that the photocatalytic rate of the prepared g-C_3N_4/TiO_2 photocatalyst to degrade AO7 was about three times than that of pristine TiO_2 and g-C_3N_4. The g-C_3N_4/TiO_2 composite with a ratio of 1:4 had the highest degradation efficiency for AO7 solution. Its degradation efficiency under acidic conditions was significantly higher than that under alkaline conditions. The enhancement of photocatalytic activity can be attributed to the formation of heterojunctions between g-C_3N_4 and TiO_2, which leads to rapid charge transfer and the efficient separation of photogenerated electron-hole pairs. The recycling experiment indicated that the photocatalyst of g-C_3N_4/TiO_2 nanocomposites still maintained good photochemical stability and recyclability after five cycles; this finding was important for its practical applications. A series of free radical trapping experiments showed that $\bullet O_2^-$ played a crucial role in the degradation of AO7.

Keywords TiO_2 · g-C_3N_4 · g-C_3N_4/TiO_2 · Photocatalytic · Degradation

Introduction

Photocatalytic technology is one of the most effective methods for wastewater treatment because of its low investment cost, mild reaction conditions, and negligible secondary pollution to the environment (Perera et al. 2012; Guo et al. 2014; Huo et al. 2015; Wang et al. 2017a, b). The preparation of photocatalysts with high photocatalytic activity and photochemical stability is the key factor restricting the practical applications of semiconductor photocatalysts (Tong et al. 2012; Lang et al. 2014). Among well-known photocatalysts, TiO_2 has great photocatalytic properties, long-term stability, non-toxicity, chemical inertness, and low cost; thus, this photocatalyst has been widely used in photocatalytic studies (Schneider et al. 2014; Thirugnanam et al. 2014). However, some serious shortcomings still occur. For example, TiO_2 has a large band gap (the rutile and anatase phases are 3.03 and 3.20 eV, respectively), which can absorb only ultraviolet light (approximately 5% of solar light). Meanwhile, its photogenerated electron-hole pairs are easy to recombine. Thus, the efficiency for charge separation needs to be further improved. Many researchers focused on the modification of TiO_2 to obtain new types of highly active photocatalysts that can work under visible light (Pelaez et al. 2012; Banerjee et al.

Responsible editor: Suresh Pillai

✉ Guangzhou Qu
qugz@nwsuaf.edu.cn

[1] College of Natural Resources and Environment, Northwest A&F University, Yangling 712100, Shaanxi, People's Republic of China

[2] Key Laboratory of Plant Nutrition and the Agri-environment in Northwest China, Ministry of Agriculture, Yangling 712100, Shaanxi, People's Republic of China

[3] Key Laboratory of Jiangxi Province for Persistent Pollutants Control and Resources Recycle, Nanchang Hangkong University, Nanchang 330063, Jiangxi, People's Republic of China

2014; Leong et al. 2014; Bu et al. 2015; Wang et al. 2015). Many attempts have been performed to enhance the visible light photocatalytic efficiency of TiO_2, including metal or non-metal doping (Kim et al. 2004; Liu et al. 2008; Zhang et al. 2011; Devi and Kavitha 2013), dye sensitization (Huang et al. 2010), surface modification (Wooh et al. 2015), and coupling with other semiconductor materials (Xie et al. 2010; Ismail et al. 2016; Sheng et al. 2016). Among these methods, the coupling of TiO_2 with guest semiconductors is an effective way to improve its photocatalytic activity under visible light.

Graphite carbon nitride (g-C_3N_4), which is an emerging non-metallic semiconductor photocatalyst, has attracted increasing interest due to its good visible light response, narrow band gap (about 2.70 eV), non-metallicity, non-toxicity, chemical stability, and excellent photocatalytic activity. It has been widely used in the fields of dye wastewater treatment (Xiao et al. 2015), antibiotic degradation (Panneri et al. 2017), and decomposition of water to hydrogen (Naseri et al. 2017). However, given its small specific surface area and rapid recombination of photogenerated electron-hole pairs, the usage of g-C_3N_4 in the photocatalysis field is still limited (Dong et al. 2015; Ye and Chen 2016). Previous studies showed that the coupling of g-C_3N_4 with a semiconductor having a high positive conduction band (CB) improved the catalytic activity of the newly generated photocatalyst (Kumar et al. 2013; Yang et al. 2015). Through the coupling of g-C_3N_4 with other semiconductors, photoinduced electrons are transferred to the band gap of the coupled semiconductor, thus suppressing the recombination of electrons and holes. Therefore, coupling TiO_2 with g-C_3N_4 (g-C_3N_4/TiO_2) is expected to be a good candidate for improving the separation efficiency of photogenerated electron-hole pairs and enhancing photocatalytic activity because of the variation in the band edge position of the composites. Actually, the successful synthesis of g-C_3N_4/TiO_2 composite photocatalysts has been reported in some studies. Results showed that the coupling between TiO_2 and g-C_3N_4 was effective for improving photocatalytic activity. Miranda et al. (2013) prepared the hybrid structure of g-C_3N_4 and TiO_2 by the impregnation method, which can degrade phenol under UV irradiation. Raziq et al. (2015) synthesized different mass ratios of effectively contacted TiO_2/bulk g-C_3N_4 composites by a wet chemical method and evaluated their photocatalytic activities for degrading acetaldehyde. Li et al. (2016) successfully prepared g-C_3N_4/TiO_2 composite photocatalyst by an acetic acid assisted sol-gel method combined with calcination process, which extended light absorption wavelength and enhanced photocatalytic performance. To date, the methods used to prepare g-C_3N_4/TiO_2 composite photocatalysts are numerous, but there is less satisfactory method that is widely recognized. Therefore, the search for a simple and effective synthesis method to improve its photocatalytic activity is necessary for its practical application.

In this study, g-C_3N_4/TiO_2 heterostructured photocatalysts with high activity were in situ synthesized by simple ultrasonic mixing and calcination by using TiO_2 and melamine as raw materials. The phase composition and morphology of the prepared g-C_3N_4/TiO_2 heterojunction photocatalyst were investigated by field emission scanning electron microscopy (FESEM), transmission electron microscopy (TEM), X-ray diffraction (XRD), Fourier-transform infrared spectroscopy (FT-IR), UV-Vis diffuse reflectance spectroscopy (UV-Vis DRS), and X-ray photoelectron spectroscopy (XPS). The photocatalytic activity of g-C_3N_4/TiO_2 heterostructured photocatalysts to degrade Orange II (AO7) solution under visible light was evaluated. A possible reaction mechanism was also proposed.

Experimental

Materials

Titanium (IV) oxide (TiO_2, ≥ 98%, CP grade) was purchased from Sinopharm Chemical Reagent Co. Ltd. (Shanghai, China). Melamine ($C_3H_6N_6$, ≥ 99.5%, AR grade) as a precursor of g-C_3N_4 was obtained from Tianjin Kemiou Chemical Reagent Co. Ltd. AO7 ($C_{16}H_{11}N_2NaO_4S$, > 85%) was supplied from Shanghai Aladdin Biochemical Technology Co. Ltd. Other chemicals were obtained from Tianjin Kermel Reagent Co. Ltd. (China) and were analytical grade. All chemicals were used without further purification.

Preparation of photocatalysts

The g-C_3N_4/TiO_2 nanocomposites were prepared by a simple two-step method. First, 1.0-g TiO_2 and a certain amount of melamine (1.0, 3.0, 4.0, and 5.0 g) were dispersed together in 20-ml deionized water. The suspension solution was under ultrasonic treatment for 60 min. The obtained mixed solution was dried at 60 °C in an oven. Finally, the dried samples were ground into powders before being calcined at 450 °C for 240 min in the crucible covered by a lid. After cooling to room temperature, the resultant yellow lumps were ground into powders for further use.

The synthesized composites were denoted as *x*:*y* g-C_3N_4/TiO_2, where *x*:*y* meant the weight ratio of TiO_2 and melamine. For comparison, pristine TiO_2 and melamine powders were also treated using the above method; the powders were denoted as TiO_2 and g-C_3N_4, respectively. Meanwhile, a mixing sample with the same mass ratios of g-C_3N_4 to TiO_2 was

prepared by a simple mechanical mixing of TiO_2 and g-C_3N_4, which was noted as "physical mixing."

Characterization

The structure and phase characterization of the prepared samples were performed by XRD (Bruker D8 Advance, Germany). The surface morphologies was observed by FESEM (Hitachi S-4800, Japan), whereas the microstructures were obtained using TEM (FEI Tecnai G2 spirit, Holland). FT-IR (Nicolet IS5, USA) was used to analyze the composition information and chemical bonds of the samples. The optical properties of the samples were investigated using UV-Vis DRS (Shimadzu UV-2600, Japan). XPS (EscaLab 250Xi, USA) was used to determine the surface chemical compositions of the photocatalysts.

Photocatalytic experiment

The photocatalytic activities of g-C_3N_4/TiO_2 composites under visible light irradiation were investigated by the degradation effect of the AO7 solution. The light source was a 30-W visible light lamp. In a typical experiment, a 200.0-mg catalyst was completely dispersed in a 500 ml (10.0 mg/L) AO7 solution. Before turning on the light, the suspension was magnetically stirred for 60 min in the darkness to achieve the absorption-desorption equilibrium of AO7 on the g-C_3N_4/TiO_2 composites surface. At a certain time interval, 5-ml suspensions were taken, and the catalyst powders were removed by filtration through a 0.22-μm filter and then measured at 486 nm by using a UV-Vis spectrophotometer.

Results and discussion

Characterization of g-C_3N_4/TiO_2 composite photocatalysts

To understand the crystal structure of TiO_2, g-C_3N_4, and g-C_3N_4/TiO_2, the samples were first characterized by XRD. As shown in Fig. 1, the XRD pattern of TiO_2 showed evident peaks at 25.3°, 37.8°, 48.0°, 53.9°, 55.1°, and 62.7°, which corresponded to (1 0 1), (0 0 4), (2 0 0), (1 0 5), (2 1 1), and (2 0 4) of the crystal facet of anatase TiO_2 (JCPDS No. 21-1272), respectively. The weak diffraction peak at 27.4° (1 1 0) indicates the presence of small amounts of rutile phase in TiO_2. It is worth mentioning that the anatase-rutile biphasic structure could exhibit higher photocatalytic activity than their respective neat phases (Kumar and Rao 2016). Two typical diffraction peaks at 13.2° and 27.4° were detected in the XRD pattern of g-C_3N_4, corresponding to the (1 0 0) and (0 0 2) planes of g-C_3N_4, which are attributed to the in-plane structure of tri-s-triazine units and the interlayer stacking of conjugated

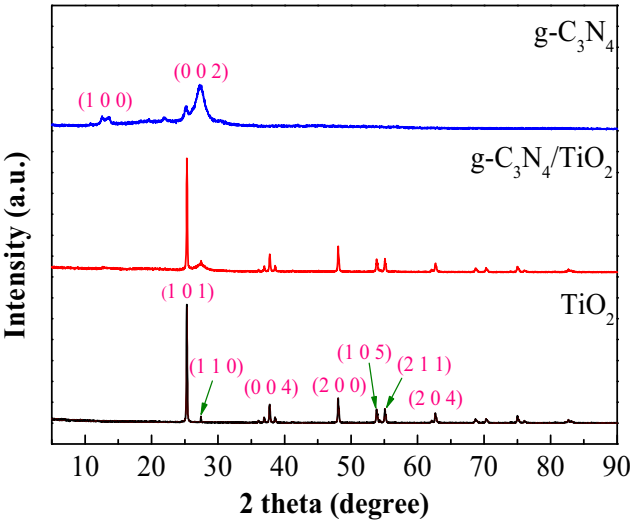

Fig. 1. XRD patterns of TiO_2, g-C_3N_4, and g-C_3N_4/TiO_2 composite

aromatic groups, respectively (Yan et al. 2009; Liang et al. 2015). g-C_3N_4 and anatase TiO_2 peaks could be observed in the g-C_3N_4/TiO_2 sample, thus indicating that the g-C_3N_4/TiO_2 composite was successfully synthesized. Furthermore, it is noteworthy that the diffraction peak of the g-C_3N_4 (0 0 2) plane overlaps the characteristic peak of the TiO_2 (1 1 0) plane rutile phase. Compared with the diffraction peaks of pristine g-C_3N_4 and TiO_2, the diffraction peak corresponding to the g-C_3N_4 (0 0 2) crystal plane in the composite is relatively broader, and the intensity is weaker. This finding can be attributed to the reduced g-C_3N_4 content in the composite.

The surface morphologies of TiO_2, g-C_3N_4, and g-C_3N_4/TiO_2 composite were observed by SEM. As seen from Fig. 2a, the pristine g-C_3N_4 displayed the typical lamellar stacking structure consisting of thin, continuous, and wrinkle-enriched g-C_3N_4 nanosheets. As shown in Fig. 2b, neat TiO_2 comprised irregular aggregates of particles. For the g-C_3N_4/TiO_2 composite, the surface of g-C_3N_4 nanosheets was obviously roughened after loading the TiO_2 particles (Fig. 2c). To further confirm whether the composite of g-C_3N_4 and TiO_2 was prepared successfully, the microstructure morphologies of TiO_2, g-C_3N_4, and g-C_3N_4/TiO_2 were characterized by TEM. As shown in Fig. 2d, e, a large amount of irregular TiO_2 particles were agglomerated, and g-C_3N_4 is an obvious lamellar structure, consistent with the results obtained by SEM. It can also be seen from Fig. 2f that dark particles and gray areas exist. Dark particles belong to TiO_2, whereas gray areas are assigned to g-C_3N_4. This finding confirms that the TiO_2 particles are wrapped inside the g-C_3N_4 flakes. Moreover, TiO_2 particles were well dispersed on g-C_3N_4, indicating that the presence of g-C_3N_4 suppressed the aggregation of TiO_2 nanoparticles. EDX was used to investigate the composition of the g-C_3N_4/TiO_2 composite. As shown in Fig. 2g, the peaks confirmed that the product consisted of only C, N, O, and Ti elements. The above results can fully

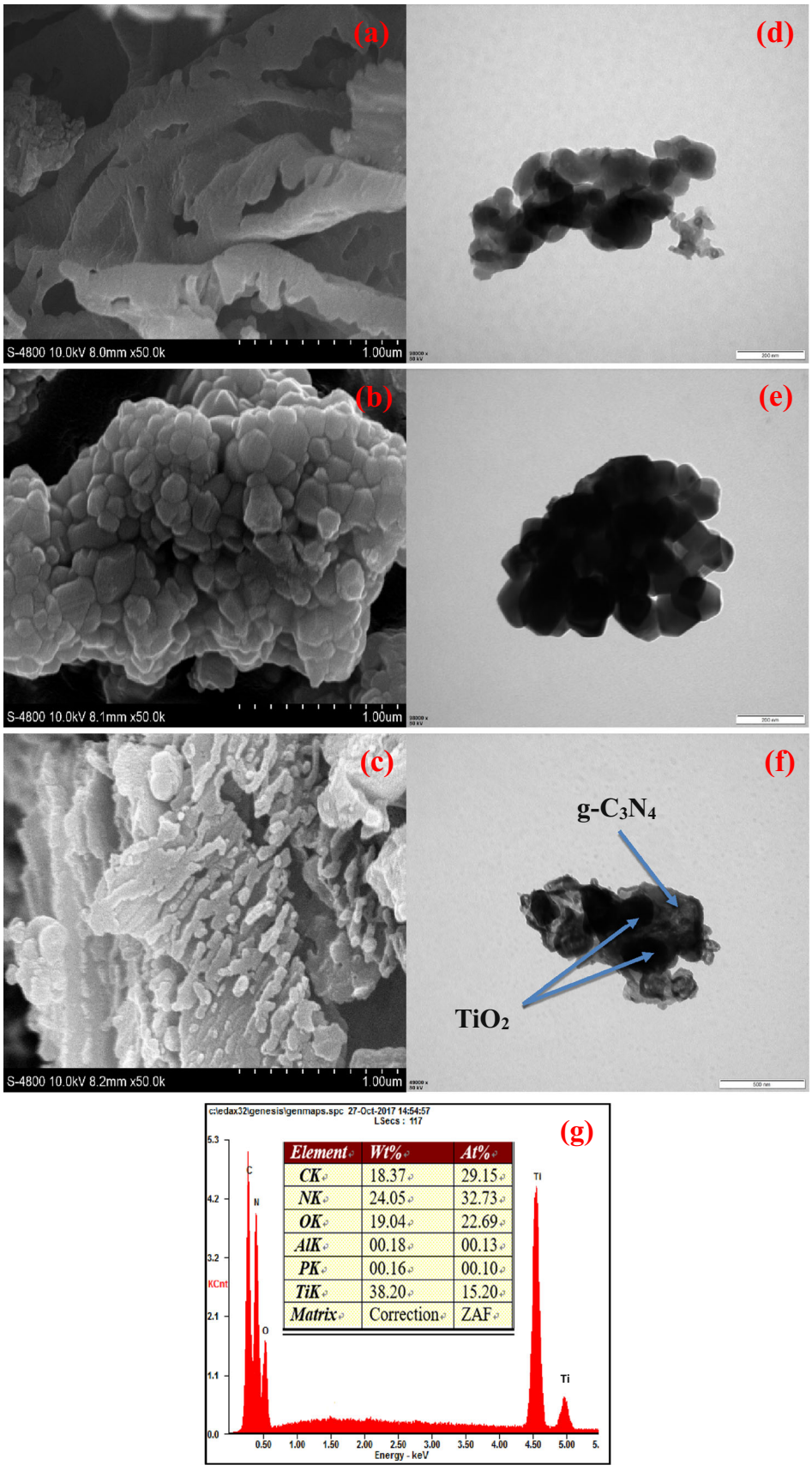

Fig. 2. SEM images of g-C_3N_4 (**a**), TiO_2 (**b**), and g-C_3N_4/TiO_2 composite (**c**). TEM images of g-C_3N_4 (**d**), TiO_2 (**e**), and g-C_3N_4/TiO_2 composite (**f**). EDX spectrum of g-C_3N_4/TiO_2 composite (**g**)

demonstrate that the g-C_3N_4/TiO_2 heterojunction photocatalyst was successfully synthesized.

The compositional information and chemical bonds of TiO_2, g-C_3N_4, and g-C_3N_4/TiO_2 composite were analyzed by FT-IR spectroscopy. As shown in Fig. 3, the main peaks at 400–700 cm^{-1} for neat TiO_2 are attributed to Ti—O—Ti and Ti—O stretching vibration modes in anatase TiO_2 crystals (Wu et al. 2016). The broad peak at 3000–3300 cm^{-1} for pristine g-C_3N_4 corresponds to the stretching mode of the terminal NH_2 of the NH groups at the defect sites of the aromatic rings, whereas several peaks in the 1200–1650-cm^{-1} range are assigned to the typical stretching mode of C—N heterocycles (Zhang et al. 2012). Furthermore, the sharp peak at 810 cm^{-1} is attributed to the characteristic breathing mode of tri-s-triazine units (Lotsch and Schnick 2006). Given that most characteristic peaks of g-C_3N_4 and TiO_2 were observed, the existence of TiO_2 and g-C_3N_4 in g-C_3N_4/TiO_2 composites can be further confirmed.

The g-C_3N_4/TiO_2 composite was further characterized by XPS to study the surface chemical composition and chemical state of the elements. As shown in Fig. 4a, the signals of C, N, O, and Ti were detected in the survey XPS spectrum of the g-C_3N_4/TiO_2 composite. No peaks of other elements were found, which indicated that the g-C_3N_4/TiO_2 heterojunction photocatalyst was mainly composed of C, N, O, and Ti elements; this consequence was in agreement with the result of EDX (Fig. 2g). As illustrated in Fig. 4b, the Ti 2p spectra of the g-C_3N_4/TiO_2 composite have two peaks at 458.6 and 464.3 eV, corresponding to Ti $2p_{3/2}$ and Ti $2p_{1/2}$, respectively (Li et al. 2015). Figure 4c showed a high-resolution C 1s spectrum of the g-C_3N_4/TiO_2 composite having two C 1s peaks at 284.6 and 288.1 eV. The former peak corresponds to the C—C coordination, which could be explained by the reason of the accidental hydrocarbon of the XPS instrument itself and the sp^2 hybridized carbon atoms of g-C_3N_4 (Ye et al. 2011). The latter peak is assigned to the N—C=N coordination of sp^3 bonding (Singh et al. 2012). The high-resolution peak fitting spectra of N 1s was displayed in Fig. 4d. Three peaks at 398.6, 399.3, and 401.2 eV correspond to sp^2 hybridized nitrogen (C=N—C), tertiary nitrogen (N—C_3), and C—N—H, respectively (Chen et al. 2014). The O 1s high-resolution spectra of the g-C_3N_4/TiO_2 composite were fitted to two peaks at 529.8 and 532.1 eV in Fig. 4e, corresponding to Ti—O bond and O—H bond, respectively (da Silva et al. 2000).

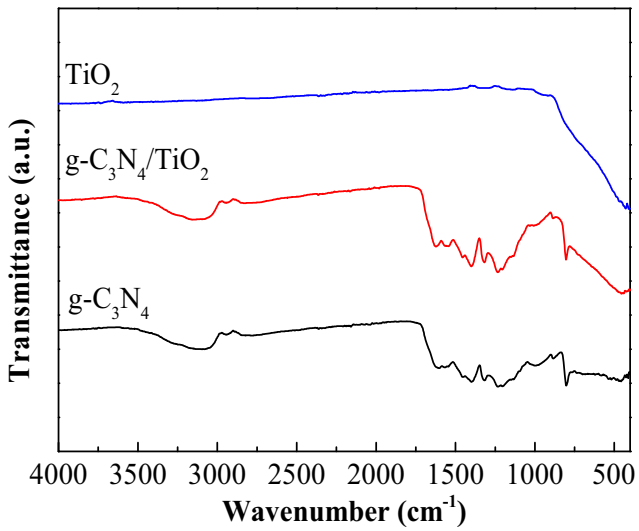

Fig. 3. FT-IR spectra of TiO_2, g-C_3N_4, and g-C_3N_4/TiO_2 composite

The optical properties of TiO_2, g-C_3N_4, and g-C_3N_4/TiO_2 composite were subsequently studied by using UV-Vis DRS spectroscopy. As shown in Fig. 5a, the absorption edges of pristine TiO_2 and g-C_3N_4 were approximately 380 and 460 nm in the visible region, respectively, agreeing well with the theoretical value (Tong et al. 2015). In comparison with TiO_2, the absorption edge of the g-C_3N_4/TiO_2 composite obviously red shifted to the visible region in the range of 320–700 nm. Even though pristine g-C_3N_4 presented better absorbency and absorption edge range than the g-C_3N_4/TiO_2 composite, many factors still affect the photocatalytic activity of photocatalysts. It cannot be simply considered that the improved visible light absorption can increase catalytic activity under visible light irradiation. The existence of TiO_2 here is expected to produce effective interfacial electron transfer, which is helpful for the electron-hole pair separation of g-C_3N_4 and the enhancement of catalytic activity under visible light irradiation. As shown in Fig. 5b, the band gap energies of the direct transition semiconductors were estimated by plots of $(\alpha h\nu)^{1/2}$ vs photon energy on the basis of the following formula (Chen et al. 2016):

$$(\alpha h\nu)^{1/2} = A\left(h\nu - E_g\right) \quad (1)$$

where α, h, ν, A, and E_g represent the absorption coefficient, Planck's constant, optical frequency, constant, and band gap, respectively. It can be estimated from Fig. 5b that the band gap energies of pristine TiO_2 and g-C_3N_4 were 3.05 and 2.70 eV, respectively, which was consistent with the previous report (Yan and Yang 2011). However, the band gap of the g-C_3N_4/TiO_2 composite was greatly reduced to 2.60 eV. These results fully demonstrated that the electronic structure of TiO_2 in the g-C_3N_4/TiO_2 composite may be changed by introducing g-C_3N_4, which narrows the band gap of the composite.

Photocatalytic activity and influential factors

The photocatalytic activities of photocatalysts with different structures were evaluated by investigating the degradation of AO7 solution. As shown in Fig. 6a, the photolysis of the AO7 solution was neglected without the aid of photocatalysts, thus indicating that illumination and

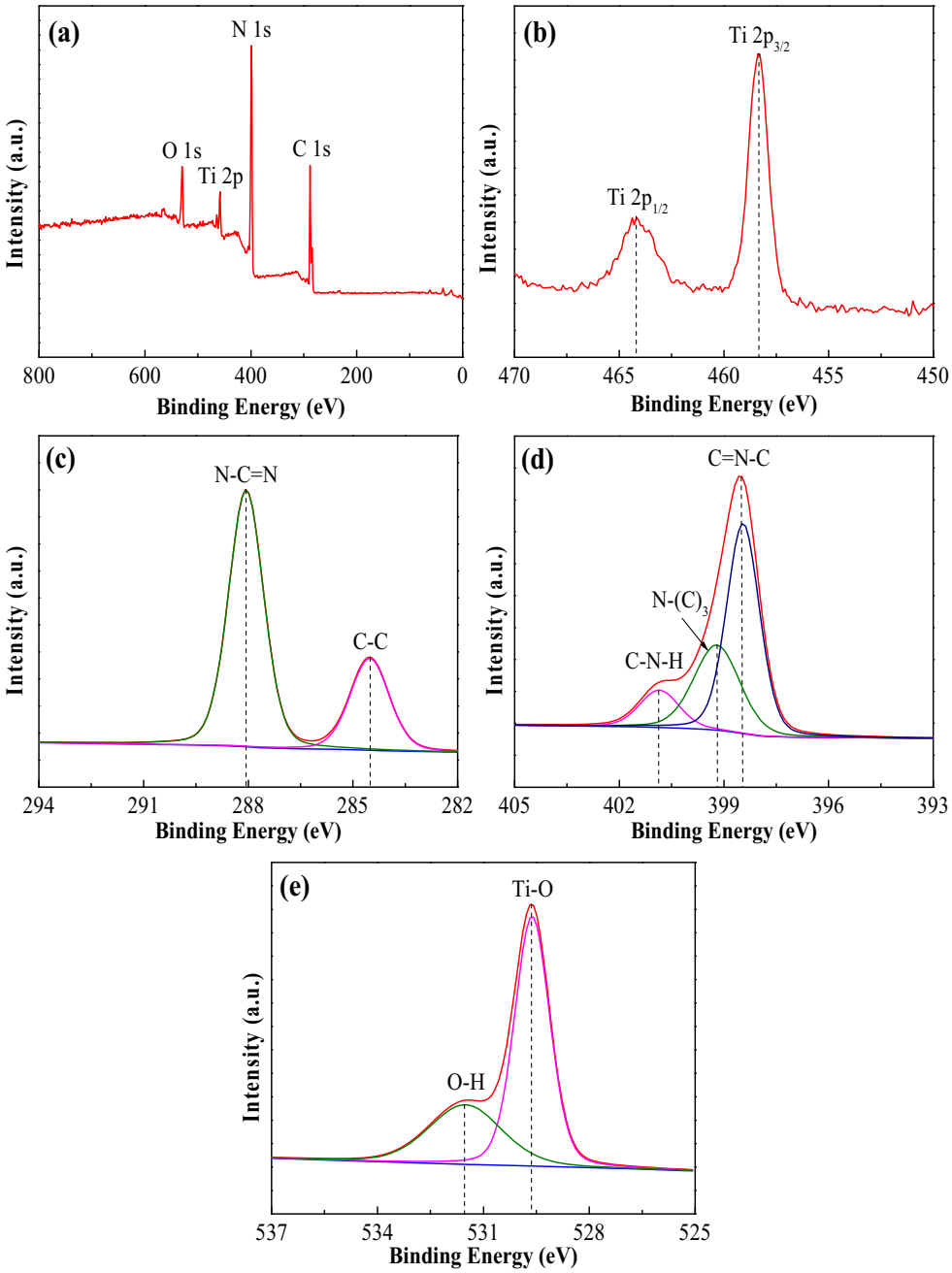

Fig. 4. XPS spectra of the g-C_3N_4/TiO_2 composite: survey spectrum (**a**), Ti 2p (**b**), C 1s (**c**), N 1s (**d**), and O 1s (**e**)

stirring negligibly affected its degradation. Given that pristine TiO_2 showed weaker absorbance at 365 nm than g-C_3N_4 and the g-C_3N_4/TiO_2 composite, as evidenced by UV-Vis DRS (see Fig. 5a), weak photocatalytic activity was achieved. Although neat g-C_3N_4 had high absorbance at 365 nm, the easy recombination of electron-hole pairs resulted in low photocatalytic activity. For the "physical mixing" sample, the photocatalytic activity was lower than that of g-C_3N_4/TiO_2, although the same mass ratio was shared. No chemical bond existed in the simply physically mixed sample to create a large void between TiO_2 and g-C_3N_4, thus limiting the transfer of photogenerated electrons and resulting in a high recombination of electron-hole pairs (Chen et al. 2016). It is no difficult to find that the g-C_3N_4/TiO_2 composite shows higher photocatalytic activity than other photocatalysts. The possible reason for this is the close connection of TiO_2 and g-C_3N_4 in the g-C_3N_4/TiO_2 composite. The photoresponse range of TiO_2 is broadened in the presence of g-C_3N_4, and the photogenerated electrons and holes are separated effectively.

To investigate the effects of calcination temperature on the photocatalytic activity of the composite, a series of g-C_3N_4/TiO_2 composites were prepared under different temperatures.

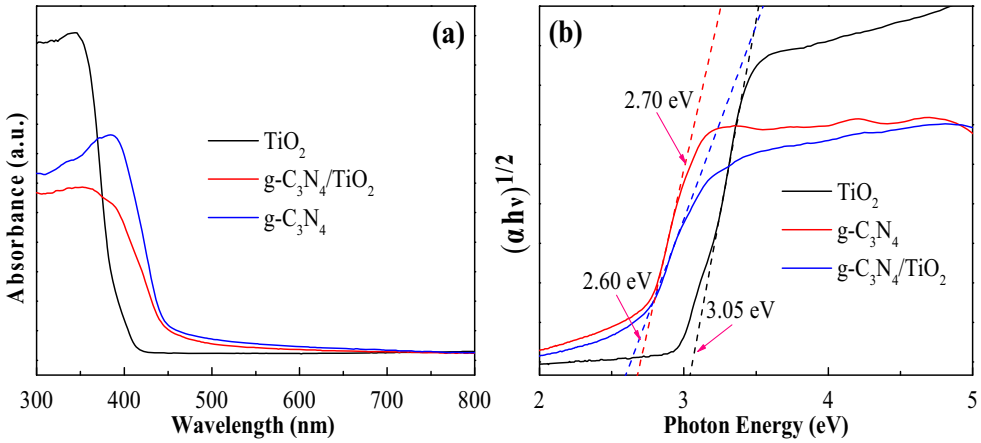

Fig. 5. UV-Vis spectra (**a**) and plots of $(\alpha h\nu)^{1/2}$ vs photon energy (**b**) of TiO_2, g-C_3N_4, and g-C_3N_4/TiO_2 composite

As can be seen from Fig. 6b, the photocatalytic activity of composites increased first and decreased later with the rise of temperatures. In particular, the composites prepared at 450 °C exhibited the best photocatalytic activity. With the increase in temperature, the g-C_3N_4 was gradually generated in the composites, and the photocatalytic activity increased gradually. A high temperature would lead to the thermal decomposition of g-C_3N_4, thus reducing photocatalytic activity.

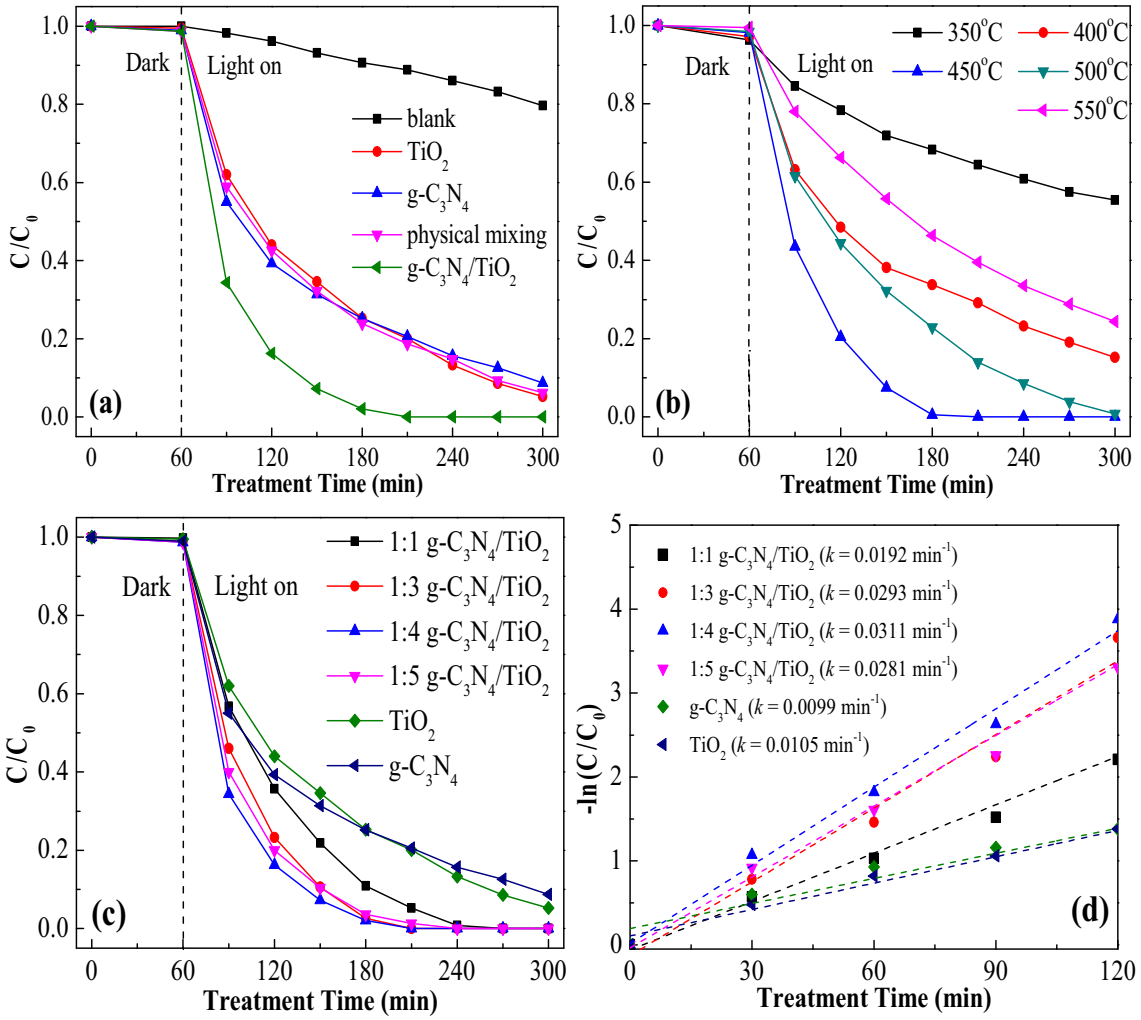

Fig. 6. Effects of different factors on the photocatalytic degradation of AO7: catalyst structure (**a**), calcination temperature (**b**), weight ratio of TiO_2 and melamine (**c**), pseudo-first-order kinetics of AO7 degradation by different catalysts having varied weight ratio of TiO_2 and melamine (**d**)

Therefore, the calcination temperature of 450 °C was selected to study the effect of the weight ratio of TiO_2 and melamine on the photocatalytic activity.

As shown in Fig. 6c, the photocatalytic activity of all *x*:*y* g-C_3N_4/TiO_2 composites was evidently higher than that of pristine TiO_2 and g-C_3N_4. The enhancement of the photocatalytic activity of *x*:*y* g-C_3N_4/TiO_2 was attributed to the heterojunction effects between g-C_3N_4 and TiO_2 as mentioned above. Meanwhile, when the mass ratio of TiO_2 and melamine increased from 1:1 to 1:4, the photocatalytic activity of g-C_3N_4/TiO_2 composites increased. The g-C_3N_4/TiO_2 composites with a ratio of 1:4 exhibited the highest photocatalytic activity. The further raising the melamine ratio increased the amount of g-C_3N_4 produced in the composite. However, the degradation rate of AO7 decreased. Thus, only proper g-C_3N_4 content can promote the generation and transfer of photogenerated electrons and holes. The excess of g-C_3N_4 as a new center for the recombination of charge carriers accelerated the recombination of electron-hole pairs, thus deteriorating their photocatalytic activity.

The catalytic rates of photocatalysts with different mass ratios were further analyzed by the kinetic model. The process of the photocatalytic degradation conforming to the pseudo-first-order kinetic model can be expressed as follows:

$$-\ln(C/C_0) = kt \quad (2)$$

where C_0, C, k, and t represent the initial AO7 concentration, AO7 concentration after t min irradiation, rate constant, and irradiation time, respectively (Zhang et al. 2013). The rate constants for different samples are shown in Fig. 6d The g-C_3N_4/TiO_2 composite with a ratio of 1:4 exhibited excellent photocatalytic activity. The rate constant $k = 0.0311$ min^{-1} of the reaction was about three times than that of pristine g-C_3N_4 ($k = 0.0099$ min^{-1}) and TiO_2 ($k = 0.0105$ min^{-1}). It is further confirmed that TiO_2 and g-C_3N_4 connected by heterojunction can highly improve the photocatalytic reaction rate.

The effect of catalyst dosage on the degradation efficiency of AO7 was shown in Fig. 7a. The degradation efficiency of the AO7 solution increased with the amount of the g-C_3N_4/TiO_2 composite. When the amount of photocatalyst reached 200.0 mg, the degradation efficiency of the AO7 solution reached saturation. With the increasing amount of photocatalyst, the generated active sites increased, thus facilitating the adsorption of pollutants and increasing photocatalytic activity. When the catalyst was added excessively, the absorption of light by the photocatalyst was saturated. As a result, the photocatalytic activity remained the same.

The pH of the solution can affect the charge distribution on the surface of photocatalysts, which plays an important role in the photocatalytic reaction. Figure 7b shows the effect of pH on the photocatalytic degradation of the AO7 solution. The photocatalytic activity of the g-C_3N_4/TiO_2 composite varied under acidic (pH = 4) and basic (pH = 11) conditions and decreased with an increase in pH value. The point of zero charge (PZC) may exist in the g-C_3N_4/TiO_2 composite. When the solution pH was lower than PZC, the g-C_3N_4/TiO_2 composite was positively charged. Therefore, negatively charged AO7 molecules were absorbed on g-C_3N_4/TiO_2 composites, and AO7 degradation efficiency was improved. By contrast, when the solution pH was higher than PZC, the g-C_3N_4/TiO_2 composite and AO7 molecules were negatively charged, resulting in electrostatic repulsion. Thus, the degradation efficiency was reduced (Li et al. 2017).

The photostability and recyclability of photocatalysts are critical for their practical application. Therefore, recycling experiments were conducted five times to evaluate the stability and reusability of the g-C_3N_4/TiO_2 composite. As shown in Fig. 8, the photocatalytic activity of the g-C_3N_4/TiO_2 composite almost remained the same after five cycles, thus indicating

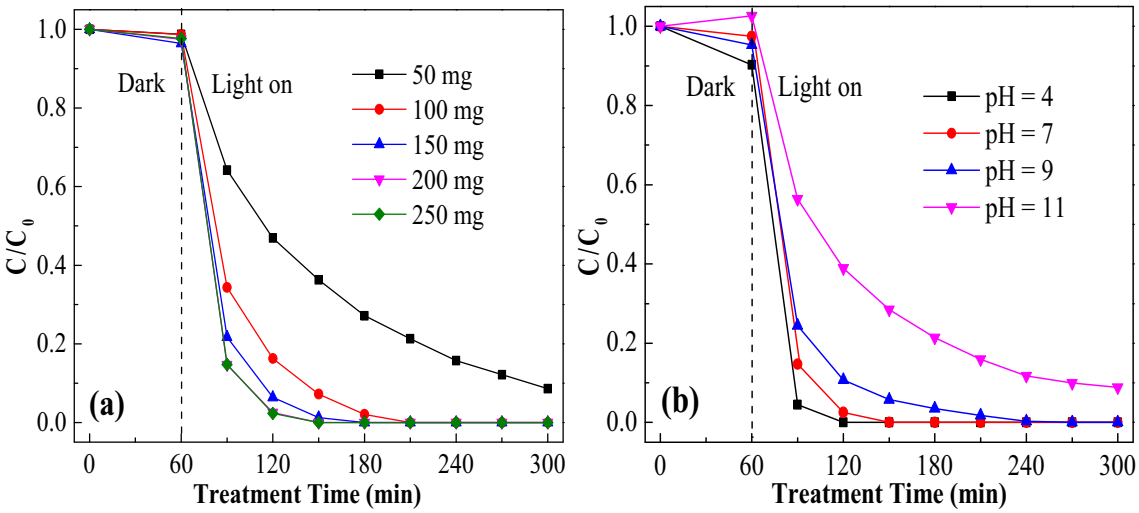

Fig. 7. Effects of different factors on the photocatalytic degradation of AO7: catalyst dosage (**a**), pH (**b**)

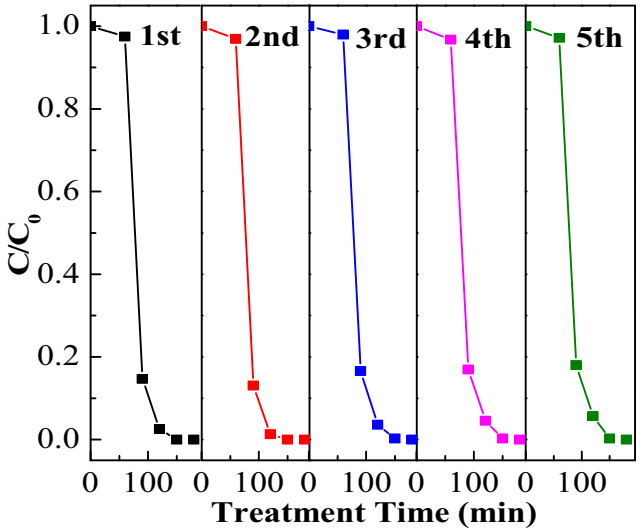

Fig. 8. The photostability and recyclability of g-C_3N_4/TiO_2 composites to the photocatalytic degradation of AO7

that the composite presented good photostability and recyclability.

Photocatalytic mechanism

Figure 9 displays the variation in the UV-Vis absorption spectra of the AO7 solution degraded by the g-C_3N_4/TiO_2 composite at different times. The main absorption peak of AO7 solution is approximately at 486 nm, which originates from the azo bond. The intensity of the peak decreased with time (Zhou et al. 2016). The disappearance of the peak at 486 nm after the light irradiation for 150 min indicated that the AO7 solution was completely discolored. Figure 9b shows the changes in the COD value of solution at different treatment times. It can find that the COD removal rate only is 48% at 150 min. With the progress of the photocatalytic reaction, the removal rate of COD continues to increase. At 300 min, the COD removal rate can reach 93%, indicating that there is still a portion of the intermediate organics in the wastewater. The reason may be that AO7 dye wastewater is not directly mineralized into CO_2 and H_2O during the photocatalytic degradation process. It is degraded into some intermediate products through degradation of chromophoric groups and benzene-like ring structure and then degraded into CO_2 and H_2O. These results further confirmed that the prepared g-C_3N_4/TiO_2 composite can degrade AO7 in solution under visible light.

Generally, $^{\cdot}OH$, h^+, and $^{\cdot}O_2^-$ are considered active radicals that play major roles in photocatalytic reaction. To verify the existence of these three reactive free radicals and analyze their roles in the degradation of AO7, a series of free radical trapping experiments were performed. Isopropyl alcohol (IPA), p-benzoquinone (p-BQ), and ammonium oxalate (AO) were used as scavengers for $^{\cdot}OH$, $^{\cdot}O_2^-$, and h^+, respectively. As shown in Fig. 10, when IPA and AO were added into the reaction system, the degradation rate of AO7 decreased from 85.32 to 78.01 and 83.42%, respectively. However, when p-BQ was added, the photocatalytic activity was greatly inhibited, and the degradation rate of AO7 was reduced to 39.03%. Therefore, it can be considered that $^{\cdot}O_2^-$ was the main active material in the photocatalytic degradation processes of AO7 using the g-C_3N_4/TiO_2 composite, whereas the effect of h^+ was negligible.

On the basis of the above analysis and related literature reports, the mechanism of the photocatalytic reaction of the g-C_3N_4/TiO_2 composite was proposed and illustrated schematically in Fig. 11. The potentials of valence band (VB) and CB of a semiconductor material can be estimated according to Eqs. (3) and (4) (Zhang et al. 2016):

$$E_{VB} = \chi - E_e + 0.5E_g \quad (3)$$

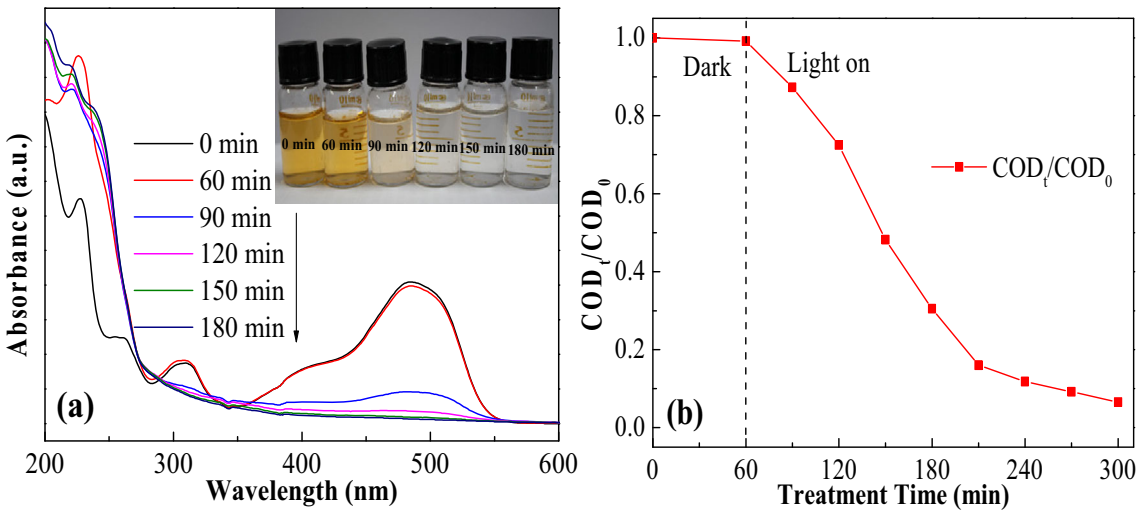

Fig. 9. The UV-Vis absorption spectra changes of the AO7 solution at different irradiation times with the g-C_3N_4/TiO_2 composite (**a**). The change of COD in solution at different treatment times (**b**)

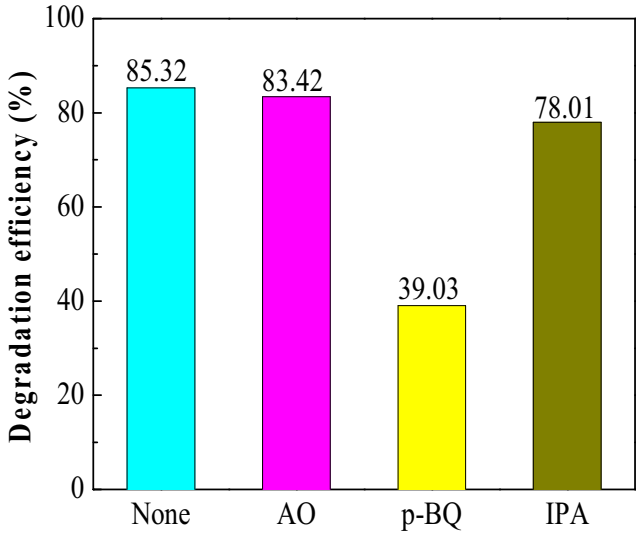

Fig. 10. Effects of different scavengers on the photocatalytic degradation of AO7

$$E_{CB} = E_{VB} - E_g \quad (4)$$

where E_{VB} and E_{CB} are the VB edge potential and CB edge potential, respectively; χ is the electronegativity of the semiconductor, which is the geometric mean of the constituent atoms. E_e is the energy of free electrons with the hydrogen scale (4.5 eV vs NHE), and E_g is the band gap energy of the semiconductor. The χ values of TiO_2 and g-C_3N_4 are 5.81 and 4.73 eV, respectively (Hao et al. 2016). The E_{CB} and E_{VB} of TiO_2 are − 0.21 and 2.84 eV, respectively, as estimated from the results of UV-Vis DRS (see Fig. 5) and Eqs. (3) and (4); the E_{CB} and E_{VB} of g-C_3N_4 are − 1.12 and 1.58 eV, respectively. Low et al. (2017) reported that the heterojunction photocatalysts belong to type-II with a staggered gap if the CB and the VB levels of semiconductor A are higher than the corresponding levels of the semiconductor B. Therefore, it can confirm that the g-C_3N_4/TiO_2 composite is of type-II heterojunction. The photogenerated electrons of g-C_3N_4 will transfer to semiconductor TiO_2 under light irradiation and resulting in a spatial separation of electron-hole pairs. Under light irradiation, g-C_3N_4 absorbed both visible and UV light, whereas TiO_2 absorbed only UV light and electrons transited from their VB to the CB. Given that the CB of g-C_3N_4 (− 1.12 eV) is more negative than that of TiO_2 (− 0.22 eV), photogenerated electrons were transferred from the CB of g-C_3N_4 to the CB of TiO_2, whereas holes remained in the VB of g-C_3N_4. Meanwhile, the CB of both g-C_3N_4 and TiO_2 are more negative than that of $E(O_2/{}^{\cdot}O_2^-)$ (− 0.046 eV vs NHE). Therefore, the electrons on the CB of TiO_2 and the non-transferred electrons on g-C_3N_4 can capture the O_2 generation of ${}^{\cdot}O_2^-$, which was the most important active material in the photocatalytic degradation of AO7 (see Fig. 10). However, only photogenerated holes on the VB of TiO_2 can react with OH^- or H_2O to form ·OH because the potential of $E({}^{\cdot}OH/H_2O)$ (2.68 eV vs NHE) and $E({}^{\cdot}OH/OH^-)$ (1.99 eV vs NHE) is lower than the VB of TiO_2 (Wang et al. 2017a, b). Furthermore, photogenerated holes left on VB can also oxidize the organic pollutants in the solution by direct and indirect oxidation. Therefore, the rapid charge transfer was achieved through the heterojunction interface between g-C_3N_4 and TiO_2, and the difference in potential enabled the effective separation of photogenerated electron-hole pairs.

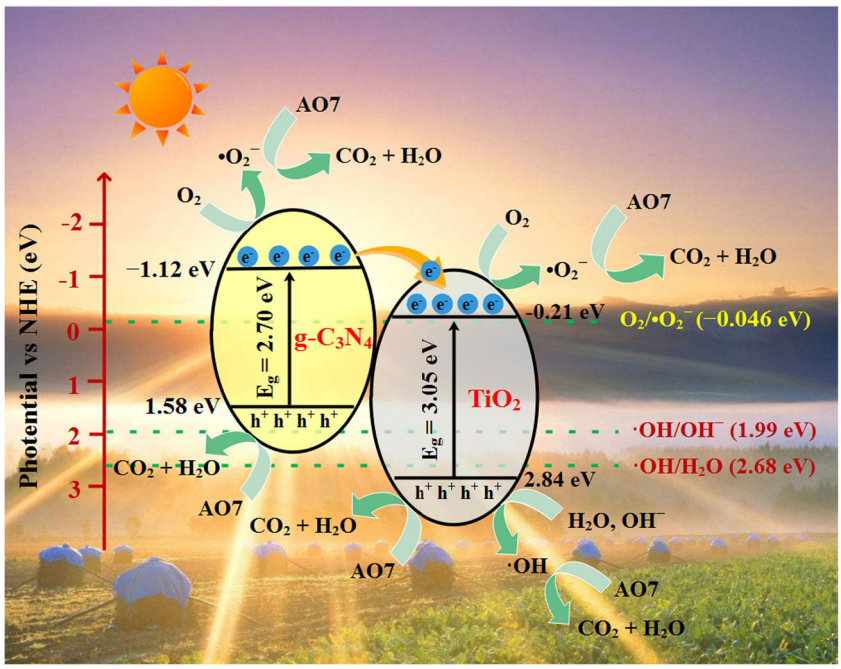

Fig. 11. Schematic diagram for the mechanism of the photocatalytic degradation of AO7 via g-C_3N_4/TiO_2 under visible light irradiation

The photocatalytic activity of the g-C_3N_4/TiO_2 composite increased greatly. The specific reactions involved in this photocatalytic process are as follows:

$$\text{Photocatalyst} + h\nu \rightarrow e^- + h^+ \quad (5)$$

$$e^- + O_2 \rightarrow \cdot O_2^- \quad (6)$$

$$h^+ + H_2O/OH^- \rightarrow \cdot OH \quad (7)$$

$$\cdot O_2^- + H_2O/H^+ \rightarrow \cdot OH \quad (8)$$

$$\cdot O_2^-/h^+/\cdot OH + AO7 \rightarrow CO_2 + H_2O \quad (9)$$

Conclusions

In summary, the g-C_3N_4/TiO_2 composite photocatalyst was successfully prepared by a simple ultrasonic mixing and calcination method. The prepared g-C_3N_4/TiO_2 composite showed higher photocatalytic activity than pristine TiO_2 and g-C_3N_4. The 1:4 g-C_3N_4/TiO_2 composite with 200.0 mg exhibited the highest degradation efficiency for 10.0 mg/L of the AO7 solution. The degradation rate of g-C_3N_4/TiO_2 to the AO7 solution under acid conditions was obviously higher than that under alkaline conditions because of the influence of pH on the charge distribution on the catalyst surface. A series of free radical trapping experiments showed that $\cdot O_2^-$ played the most important role in the degradation of AO7. The enhanced catalytic activity of the prepared g-C_3N_4/TiO_2 composites can be attributed to the formation of heterojunctions between g-C_3N_4 and TiO_2, which result in the rapid charge transfer and the efficient separation of photogenerated electron-hole pairs.

Funding information The authors gratefully acknowledge the financial support provided by the National Natural Science Foundation of China (grant no. 21107085), the Overseas Student's Science and Technology Activities Project Merit Funding of Shaanxi, the Key Laboratory of Jiangxi Province for Persistent Control and Resources Recycle (Nanchang Hangkong University, grant no. ES201780295), and the Fundamental Research Funds for the Central Universities (grant no. 2452017106).

References

Banerjee S, Pillai SC, Falaras P, O'Shea KE, Byrne JA, Dionysiou DD (2014) New insights into the mechanism of visible light photocatalysis. J Phys Chem Lett 5:2543–2554

Bu XZ, Wang Y, Li J, Zhang CH (2015) Improving the visible light photocatalytic activity of TiO_2 by combining sulfur doping and rectorite carrier. J Alloys Compd 628:20–26

Chen YF, Huang WX, He DL, Yue ST, Huang H (2014) Construction of heterostructured g-C_3N_4/Ag/TiO_2 microspheres with enhanced photocatalysis performance under visible-light irradiation. ACS Appl Mater Interfaces 6:14405–14414

Chen XF, Wei J, Hou RJ, Liang Y, Xie ZL, Zhu YG, Zhang XW, Wang HT (2016) Growth of g-C_3N_4 on mesoporous TiO_2 spheres with high photocatalytic activity under visible light irradiation. Appl Catal B-Environ 188:342–350

da Silva LA, Alves VA, de Castro SC, Boodts JFC (2000) XPS study of the state of iridium, platinum, titanium and oxygen in thermally formed $IrO_2 + TiO_2 + PtO_x$ films. Colloid Surface A 170:119–126

Devi LG, Kavitha R (2013) A review on non-metal ion doped titania for the photocatalytic degradation of organic pollutants under UV/solar light: role of photogenerated charge carrier dynamics in enhancing the activity. Appl Catal B-Environ 140–141:559–587

Dong F, Li YH, Wang ZY, Ho WK (2015) Enhanced visible light photocatalytic activity and oxidation ability of porous graphene-like g-C_3N_4 nanosheets via thermal exfoliation. Appl Surf Sc 358:393–403

Guo F, Shi WL, Lin X, Che GB (2014) Hydrothermal synthesis of graphitic carbon nitride-$BiVO_4$ composites with enhanced visible light photocatalytic activities and the mechanism study. J Phys Chem Solids 75:1217–1222

Hao RR, Wang GH, Tang H, Sun LL, Xu C, Han DY (2016) Template-free preparation of macro/mesoporous g-C_3N_4/TiO_2 heterojunction photocatalysts with enhanced visible light photocatalytic activity. Appl Catal B-Environ 187:47–58

Huang FZ, Chen DH, Zhang XL, Caruso RA, Cheng YB (2010) Dual-function scattering layer of submicrometer-sized mesoporous TiO_2 beads for high-efficiency dye-sensitized solar cells. Adv Funct Mater 20:1301–1305

Huo YN, Hou RJ, Chen XF, Yin HB, Gao Y, Li HX (2015) BiOBr visible-light photocatalytic films in a rotating disk reactor for the degradation of organics. J Mater Chem 3:14801–14808

Ismail AA, Abdelfattah I, Helal A, Al-Sayari SA, Robben L, Bahnemann DW (2016) Ease synthesis of mesoporous WO_3-TiO_2 nanocomposites with enhanced photocatalytic performance for photodegradation of herbicide imazapyr under visible light and UV illumination. J Hazard Mater 307:43–54

Kim DH, Hong HS, Kim SJ, Song JS, Lee KS (2004) Photocatalytic behaviors and structural characterization of nanocrystalline Fe-doped TiO_2 synthesized by mechanical alloying. J Alloys Compd 375:259–264

Kumar SG, Rao KSRK (2016) Comparison of modification strategies towards enhanced charge carrier separation and photocatalytic degradation activity of metal oxide semiconductors (TiO_2, WO_3 and ZnO). Appl Surf Sci 391:124–148

Kumar S, Surendar T, Baruah A, Shanker V (2013) Synthesis of a novel and stable g-C_3N_4-Ag_3PO_4 hybrid nanocomposite photocatalyst and study of the photocatalytic activity under visible light irradiation. J Mater Chem A 1:5333–5340

Lang XJ, Chen XD, Zhao JC (2014) Heterogeneous visible light photocatalysis for selective organic transformations. Chem Soc Rev 43:473–486

Leong S, Razmjou A, Wang K, Hapgood K, Zhang XW, Wang HT (2014) TiO_2 based photocatalytic membranes: a review. J Membr Sci 472:167–184

Li YL, Wang JS, Yang YL, Zhang Y, He D, An QE, Cao GZ (2015) Seed-induced growing various TiO_2 nanostructures on g-C_3N_4 nanosheets with much enhanced photocatalytic activity under visible light. J Hazard Mater 292:79–89

Li JH, Liu YL, Li HM, Chen C (2016) Fabrication of g-C_3N_4/TiO_2 composite photocatalyst with extended absorption wavelength range and enhanced photocatalytic performance. J Photoch Photobio A 317:151–160

Li TF, Wang TC, Qu GZ, Liang DL, Hu SB (2017) Synthesis and photocatalytic performance of reduced graphene oxide-TiO_2 nanocomposites for Orange II degradation under UV light irradiation. Environ Sci Pollut R 24:12416–12425

Liang QH, Li Z, Yu XL, Huang ZH, Kang FY, Yang QH (2015) Macroscopic 3D porous graphitic carbon nitride monolith for

enhanced photocatalytic hydrogen evolution. Adv Mater 27:4634–4639

Liu G, Zhao YN, Sun CH, Li F, Lu GQ, Cheng HM (2008) Synergistic effects of B/N doping on the visible-light photocatalytic activity of mesoporous TiO_2. Angew Chem Int Edit 47:4516–4520

Lotsch BV, Schnick W (2006) From triazines to heptazines: novel nonmetal tricyanomelaminates as precursors for graphitic carbon nitride materials. Chem Mater 18:1891–1900

Low JX, Yu JG, Jaroniec M, Wageh S, Al-Ghamdi AA (2017) Heterojunction photocatalysts. Adv Mater 29:1601694

Miranda C, Mansilla H, Yáñez J, Obregón S, Colón G (2013) Improved photocatalytic activity of g-C_3N_4/TiO_2 composites prepared by a simple impregnation method. J Photoch Photobio A 253:16–21

Naseri A, Samadi M, Pourjavadi A, Moshfegh AZ, Ramakrishna S (2017) Graphitic carbon nitride (g-C_3N_4)-based photocatalysts for solar hydrogen generation: recent advances and future development directions. J Mater Chem A (45):23406–23433

Panneri S, Ganguly P, Nair BN, Mohamed AAP, Warrier KGK, Hareesh UNS (2017) Role of precursors on the photophysical properties of carbon nitride and its application for antibiotic degradation. Environ Sci Pollut R 24(9):8609–8618

Pelaez M, Nolan NT, Pillai SC, Seery MK, Falaras P, Kontos AG, Dunlop PSM, Hamilton JWJ, Anthony Byrne J, O'Shea K, Entezari MH, Dionysiou DD (2012) A review on the visible light active titanium dioxide photocatalysts for environmental applications. Appl Catal B-Environ 125:331–349

Perera SD, Mariano RG, Khiem V, Nour N, Seitz O, Chabal Y, Balkus KJ Jr (2012) Hydrothermal synthesis of graphene-TiO_2 nanotube composites with enhanced photocatalytic activity. ACS Catal 2:949–956

Raziq F, Li CM, Humayun M, Qu Y, Zada A, Yu HT, Jing LQ (2015) Synthesis of TiO_2/g-C_3N_4 nanocomposites as efficient photocatalysts dependent on the enhanced photogenerated charge separation. Mater Res Bull 70:494–499

Schneider J, Matsuoka M, Takeuchi M, Zhang JL, Horiuchi Y, Anpo M, Bahnemann DW (2014) Understanding TiO_2 photocatalysis: mechanisms and materials. Chem Rev 114:9919–9986

Sheng JG, Tong HB, Xu H, Tang C (2016) Preparation and photocatalytic activity of SnO_2@TiO_2 core-shell composites modified by Ag. Catal Surv Asia 20:167–172

Singh JA, Overbury SH, Dudney NJ, Li MJ, Veith GM (2012) Gold nanoparticles supported on carbon nitride: influence of surface hydroxyls on low temperature carbon monoxide oxidation. ACS Catal 2:1138–1146

Thirugnanam L, Kaveri S, Dutta M, Jaya NV, Fukata N (2014) Porous tubular rutile TiO_2 nanofibers: synthesis, characterization and photocatalytic properties. J Nanosci Nanotechno 14:3034–3040

Tong H, Ouyang SX, Bi YP, Umezawa N, Oshikiri M, Ye JH (2012) Nano-photocatalytic materials: possibilities and challenges. Adv Mater 24:229–251

Tong ZW, Yang D, Xiao TX, Tian Y, Jiang ZY (2015) Biomimetic fabrication of g-C_3N_4/TiO_2 nanosheets with enhanced photocatalytic activity toward organic pollutant degradation. Chem Eng J 260:117–125

Wang X, Utsumi M, Yang YG, Li DW, Zhao YX, Zhang ZY, Feng CP, Sugiura N, Cheng JJY (2015) Degradation of microcystin-LR by highly efficient AgBr/Ag_3PO_4/TiO_2 heterojunction photocatalyst under simulated solar light irradiation. Appl Surf Sci 325:1–12

Wang QW, Dong SY, Zhang D, Yu CF, Lu J, Wang D, Sun JH (2017a) Magnetically recyclable visible-light-responsive MoS_2@Fe_3O_4 photocatalysts targeting efficient wastewater treatment. J Mater Sci 53:1135–1147

Wang W, Fang JJ, Shao SF, Lai M, Lu CH (2017b) Compact and uniform TiO_2@g-C_3N_4 core-shell quantum heterojunction for photocatalytic degradation of tetracycline antibiotics. Appl Catal B-Environ 217:57–64

Wooh S, Kim TY, Song D, Lee YG, Lee TK, Bergmann VW, Weber SA, Bisquert J, Kang YS, Char K (2015) Surface modification of TiO_2 photoanodes with fluorinated self-assembled monolayers for highly efficient dye-sensitized solar cells. ACS Appl Mater Interfaces 7:25741–25747

Wu YM, Tao L, Zhao J, Yue X, Deng WY, Li YX, Wang CY (2016) TiO_2/g-C_3N_4 nanosheets hybrid photocatalyst with enhanced photocatalytic activity under visible light irradiation. Res Chem Intermed 42:3609–3624

Xiao HH, Wang WY, Liu GG, Chen ZM, Lv KL, Zhu JJ (2015) Photocatalytic performances of g-C_3N_4 based catalysts for RhB degradation: effect of preparation conditions. Appl Surf Sci 358:313–318

Xie Y, Ali G, Yoo SH, Cho SO (2010) Sonication-assisted synthesis of CdS quantum-dot-sensitized TiO_2 nanotube arrays with enhanced photoelectrochemical and photocatalytic activity. ACS Appl Mater Interfaces 2:2910–2914

Yan HJ, Yang HX (2011) TiO_2-g-C_3N_4 composite materials for photocatalytic H_2 evolution under visible light irradiation. J Alloys Compd 509:L26–L29

Yan SC, Li ZS, Zou ZG (2009) Photodegradation performance of g-C_3N_4 fabricated by directly heating melamine. Langmuir 25:10397–10401

Yang XF, Tang H, Xu JS, Antonietti M, Shalom M (2015) Silver phosphate/graphitic carbon nitride as an efficient photocatalytic tandem system for oxygen evolution. ChemSusChem 8:1350–1358

Ye LJ, Chen SJ (2016) Fabrication and high visible-light-driven photocurrent response of g-C_3N_4 film: the role of thiourea. Appl Surf Sci 389:1076–1083

Ye JF, Liu W, Cai JG, Chen S, Zhao XW, Zhou HH, Qi LM (2011) Nanoporous anatase TiO_2 mesocrystals: additive-free synthesis, remarkable crystalline-phase stability, and improved lithium insertion behavior. J Am Chem Soc 133:933–940

Zhang L, Li X, Chang ZX, Li DL (2011) Preparation, characterization and photoactivity of hollow N, Co co-doped TiO_2/SiO_2 microspheres. Mater Sci Semicond Process 14:52–57

Zhang JS, Zhang MW, Zhang GG, Wang XC (2012) Synthesis of carbon nitride semiconductors in sulfur flux for water photoredox catalysis. ACS Catal 2:940–948

Zhang ZY, Shao CL, Li XH, Sun YY, Zhang MY, Mu JB, Zhang P, Guo ZC, Liu YC (2013) Hierarchical assembly of ultrathin hexagonal SnS_2 nanosheets onto electrospun TiO_2 nanofibers: enhanced photocatalytic activity based on photoinduced interfacial charge transfer. Nanoscale 5:606–618

Zhang X, Zhang P, Wang LJ, Gao HQ, Zhao JT, Liang CH, Hu JH, Shao GS (2016) Template-oriented synthesis of monodispersed SnS_2@SnO_2 hetero-nanoflowers for Cr(VI) photoreduction. Appl Catal B-Environ 192:17–25

Zhou GQ, Guo JY, Zhou GW, Wan XK, Shi HX (2016) Photodegradation of Orange II using waste paper sludge-derived heterogeneous catalyst in the presence of oxalate under ultraviolet light emitting diode irradiation. J Environ Sci 47:63–70